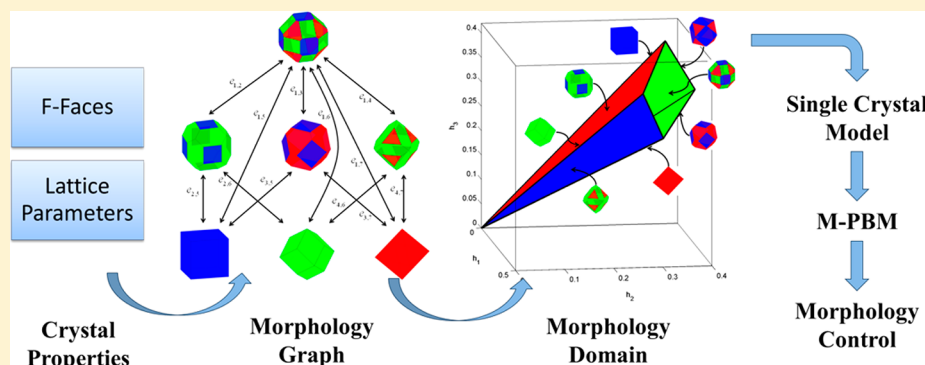# A Comprehensive Approach to Predicting Crystal Morphology Distributions with Population Balances

Meenesh R. Singh and Doraiswami Ramkrishna*

School of Chemical Engineering, Purdue University, 480 Stadium Mall Drive, West Lafayette, Indiana 47907, United States

ABSTRACT: A modeling framework is developed for predicting crystal morphology distributions with a goal toward their control in the manufacture of crystalline products. This work distinguishes itself from prior efforts in this direction by its comprehensive coverage of all possible morphologies based only on fundamental molecular information on the material. The morphology of growing crystals is composed of a finite number of low-energy faces characterized by their Miller indices and perpendicular distances. The symmetry of crystals allows the classification of kinetically and geometrically similar faces into different groups identified by their perpendicular distances (*h-vector*). A set of different kinds of morphologies obtained by combining different groups of faces is referred to as a morphology set. Further, a morphology graph is constituted with vertices as elements of morphology set and edges specifying conditions for transformations between morphologies. These conditions form a polyhedral cone, which will be called a morphology domain, in the space of *h-vectors*. The dynamics of crystal morphology is given by the trajectories of the *h-vector* inside this morphology domain. The evolution of morphology distributions due to crystal growth inside the morphology domain is described by a morphological-population balance model (M-PBM) which readily submits to solution by the method of characteristics. The methodology, illustrated in controlling crystal morphologies of potassium acid phthalate using additives, paves the way for model-based control of shape control of crystallization processes.

1. INTRODUCTION

Crystal morphology is a critical determinant of quality in commonly used crystalline materials such as pharmaceutical drugs, food products, fertilizers, specialty chemicals, cosmetics, electronics and optical materials, and so on. Ensuring quality calls for manufacturing strategies which rely on understanding of the fundamental behavior of growing crystals interacting with their environment. Their behavior depends on thermodynamic properties as well as hydrodynamic conditions in crystallizers that often lead them astray to undesirable shapes. A modeling framework is therefore essential to prohibit such errant behavior and to navigate crystals toward morphologies that cater to the demands of downstream processing or even enhancing properties concerned with their application. To show that population balances represent the ideal implement for such a framework constitutes the main objective of this article, which we do by attending to issues of formulation, solution and a demonstration for application to control.

The need for developing engineering models for prediction of morphology distributions has led researchers to formulate multidimensional population balance models (PBMs) for morphology distributions. These models are mostly confined to the simplest geometry of crystals with cursory details on their transitions which limit their applicability to real crystals. It is reasonable to sum up the current issues associated with the modeling of morphology distributions as (i) unavailability of an efficient description of morphology, (ii) high dimension of the model due to a large number of crystal faces, and (iii) accounting for morphology transformations in treating populations. The PBMs for the crystal morphologies with two or three families of faces are readily derived as the number of different kinds of morphologies is limited; however the combinatorial explosion due to larger families greatly increases the complexity in formulating PBEs. These challenges with the use of existing models call for an enhanced population balance framework accommodating the entire class of morphologies and their transformations.

In summary, the objective of this article is to develop a comprehensive framework for formulation of population balance models toward model-based control of crystal morphology distributions growing in a crystallizer. The effects of other processes such as nucleation, breakage, and agglomeration on morphology distributions are neglected here. Although we envisage general control strategies with the framework, we restrict demonstration to control using additives.

The organization of the paper is as follows. Section 2 surveys the literature on crystal morphology and their population balance modeling. Section 3 introduces the elements of morphology set, morphology graph, and morphology domain. Section 4 discusses the single crystal model. Section 5 presents the theory of morphological-PBM (M-PBM). Section 6 gives the solution of M-PBM using the method of characteristics. Section 7 demonstrates the controlled crystallization of potassium acid phthalate crystals with additives using M-PBM framework, and Section 8 summarizes the findings of this article.

2. PREVIOUS WORK

The development of crystal growth theories is mainly concerned with predicting *face-specific growth rates* and *morphologies* of crystals. (Note: the terms morphology, shape, and habit are interchangeably used in the crystallography literature and share the same meaning.) Crystal morphology is usually classified as equilibrium, steady-state, and dynamic. Equilibrium morphology is governed by the surface energies, whereas the steady-state and dynamic morphologies are dictated by the face-specific growth rates.

2.1. Equilibrium Crystal Morphology. The morphology that minimizes the total surface energy of a fixed-volume crystal is known as equilibrium crystal morphology. The formulation of equilibrium morphology was proposed independently by Gibbs[1] and by Curie.[2] Curie derived Gibbs' equilibrium condition using Gauss' principle of virtual velocities on a body subjected to capillary forces. The solution to Gibbs equilibrium was later discovered by Wulff[3] in his work on measuring relative capillary constants from classical crystal growth experiments. His theorem states that there exists a point inside an equilibrium crystal, the Wulff point, such that the perpendicular distances of tangent planes of the crystal from the Wulff point are proportional to the surface tensions along the tangent planes. The correct proofs of Wulff construction were given by Hilton,[4] Liebmann,[5] Laue,[6] and Dinghas,[7] but the proofs were specific to polyhedral shapes. The extended and more general proof was provided by Taylor,[8] showing that for any function F of surface normals there is a convex shape, the Wulff of F, which has the least surface integral for a fixed volume. The equilibrium morphologies were further classified into macroscopic and microscopic equilibrium morphologies.[9] The microscopic equilibrium considers surface and volume stresses in sub-micrometer particles, whereas macroscopic equilibrium only accounts for surface energies. Some good review articles on equilibrium morphologies are also available in the literature.[10−12] Thermodynamic equilibrium can be attained if the kinetic processes involved are sufficiently rapid to change the morphology of crystal without much increase in its mass. Smaller crystals may conform to equilibrium morphology with only slight addition of mass. However, the morphologies of larger crystals with small surface-to-volume ratio are difficult to modify in short time-scales thus impeding their rate of equilibration. In practice, crystal morphology remains far from the equilibrium and therefore governed by the kinetic processes.

2.2. Dynamic and Steady-State Crystal Morphologies. The kinetics of crystal growth is governed by the growth rates of faces. Frank[13] deduced the growth morphologies from the polar plots of distances traveled by the points on a surface along the directions of their normals. Cahn et al.[14] and Taylor et al.[15] obtained Frank's result from the characteristics of the Jacobi−Hamilton equation for surface evolution. The emergence of fans and shocks from the characteristics confirms the development of faceted morphologies during crystal growth and if the supersaturation is constant then the morphology can attain a steady state. The steady-state morphology can be obtained from the Wulff construction on the polar plot of growth rates giving morphology with perpendicular distances of faces proportional to their growth rates.[16] The faces possibly present on a crystal are the ones located at the "cusps" of the polar plots of growth rates. In most practical cases, crystals grow in diffusion-free regimes where the growth rates are proportional to the surface energies. Therefore, the most likely faces can be determined from the location of "cusps" in polar plots of surface energies. The Hartman−Perdok theory[17−19] enables the estimation of surface energies and identification low-energy faces from the calculation of periodic bond chains (PBCs). The theory classifies crystal faces into F- (flat), S- (stepped), and K- (kinked) faces based on the number of PBCs being more than one, exactly one and none, respectively. A crystal face with a higher number of PBCs will have lower energy and more stability. The faces likely to be present on crystals are therefore the F-faces and may be some of the S-faces. Besides the identification of faces that can appear during growth, their growth rates are also essential for computing dynamic and steady-state morphologies.

The fundamental theories of crystal growth rates are built on the consideration of crystal structure (Bravais[20]−Friedel[21]−Donnay−Harker[22] method), surface energies (Hartman−Perdok theory), and mechanistic processes (2D nucleation model,[23,24] Burton−Cabrera−Frank model,[25] Chernov bulk diffusion model,[26] Winn-Doherty model,[12] and MONTY[27]). The relative growth rates of the faces govern the dynamics of crystal morphology by manipulating the perpendicular distances of faces. The evolving morphology often undergoes transition caused by appearance or disappearance of faces. Johnsen[28] classified the crystal faces as "real" if they are present on a crystal and "virtual" if they can appear later. He also provided the sufficient condition for the virtual face becoming real. Borgstrom[29] and Alexandru[30] considered the effect of growth rates and the angle between the surface normals on the disappearance of faces. They introduced the concept of critical growth rates essential for real to virtual face transitions. Similar conditions were also derived for two-dimensional (2D) crystals by considering the lateral length of each face as a function of the growth rates and angle between their normals.[31,32] Prywer extensively studied the face transitions on three-dimensional (3D) crystals and developed the conditions for disappearance of rectangular faces[33] and more general conditions for arbitrary shaped faces.[34] (Note: Face transitions must not be confused with phase transitions. The former means the appearance or disappearance of faces on crystals, and the latter means appearance or disappearance of different phases such as solid, liquid, or gas.) Doherty and co-workers formulated the dynamic model for 2D crystal morphologies showing the steady state to be independent of seed morphologies[35] and dynamic model for 3D crystal morphologies considering the multifurcation of vertices into edges or faces.[36] There are some other recently

developed methods to evaluate crystal morphologies and their transformations using a set-theoretic approach,[37] Minkowski additions,[38] and vertex multifurcations.[39] Ramkrishna and co-workers[37] were the first to introduce the idea of constructing a morphology domain in h-space and address the issue of morphology transformation using a set-theoretic approach. Reinhold and Briesen[38] take a different and interesting route to describe morphology evolution of faceted and nonfaceted crystals using Minkowski sum of elementary polyhedra. Subsequently, Borchert et al.[39] performed a detailed study of the behavior of edges and vertices of crystals during morphology transformations to derive morphology domains. The latest development in modeling crystal morphologies proposed by Singh et al.[40] uses a set-theoretic approach to obtain the morphology domain, which does not involve multifurcation calculations for edges and vertices. Their method involves identification of all possible kinds of morphologies by constructing a morphology set where transformations between them are readily obtained from a morphology graph. They have introduced morphology domain as a fundamental property of crystalline materials that dictates their morphological evolution. A generalized single-crystal model that accounts for the hybrid nature of the morphology domain was developed. Their methodology comes with a general-purpose software called *MorphologyDomain*[41] to assess different morphologies and screen them using growth rate functions.

2.3. Population Balance Models for Morphology Distributions.

Morphology distributions are usually described by the number density of crystals with more than one internal coordinates. The change in number density due to crystal growth, breakage, nucleation, or aggregation is collectively described by a population balance equation (PBE).[42] Cardew[43] was the first to use PBEs to describe morphology distributions with h-vector as internal coordinates. The h-vector is a vector of perpendicular distances (h) of similar faces (a family) from center, which can be used to compute geometric quantities such as volume, area, etc. His analysis was however limited to a specific morphology and does not consider face transitions. Many crystalline materials such as hydroquinone and potassium dihyrdogen phosphate (KDP) tend to grow in rod shape which can be described using two dimensions viz. length and width. The effect of crystallization conditions on aspect ratio of hydroquinone[44] and KDP[45] crystals was studied using 2D population balance models (PBMs). The availability of advanced numerical techniques such as variants of discretization methods[46−48] and high-resolution algorithms[49] have made it possible to solve multidimensional PBMs in reasonable time.

Efforts have also been made to reduce the dimension of PBMs for computability and measurability. At fixed supersaturation, when relative growth rates are constant, the dynamic changes in h-vector can be represented by the dynamics of the h of a reference family and hence reducing the dimension of PBM to one.[50] Equivalently, under similar conditions, the dynamics of h-vector can be expressed using age of crystals which also give rise to one-dimensional (1D) PBM.[51] Briesen[52] transformed the 2D PBM of parallelepiped-shaped crystals in a length−width coordinate system to volume-shape factor coordinates. Integrating over the shape factor coordinate yielded 1D PBM in volume (measurable quantity) space, and the dynamic changes in the shape factor were inferred assuming initial Gaussian distribution of shape factors. The aforementioned transformations can only be applied to specific situations, and they may not be beneficial since the solution of such PBMs can be readily obtained, without transforming them, using the method

of characteristics.[42] Wang and co-workers[53] applied 3D PBM to potash alum where the internal coordinates are the h's of three families of faces. Subsequently, they performed principal component analysis to reduce the dimension of h-vector of potash alum which resulted in 3D PBM in principal component space.[54] In this case, there is no effective reduction in the number of internal coordinates as it is the same as the dimensions of symmetry-reduced h-vector. So far the PBMs are developed for one type of morphology and do not consider morphology transformations. Wan et al.[55] introduced an ad-hoc way to account for morphology transformations by exchanging the number distribution between different morphologies. They showed transformation of alum crystals with three families of faces to one family. Since the crystal state space for alum was not identified, the transition of crystals from three families to two families was completely missed. Ramkrishna and co-workers[37] demonstrated the construction of crystal state space for asymmetric octagonal crystals and developed coupled PBEs accounting for morphology transformations. Their framework was built for a few morphologies of asymmetric octagonal crystals and requires more generality to be applicable to other crystalline materials.

The eventual use of these models is to be able to predict and control crystal morphologies and their distributions. The identification of these models and their validation require appropriate experimental tools to measure dynamic morphologies and supersaturation. A review on process analytical technologies involved in crystallization can be found elsewhere.[56] As the flat crystals are relatively easier to measure, the PBMs for such crystals can be readily identified and control.[57−59] However, the identification of PBMs for 3D crystals requires techniques to measure their morphologies. There exist some approximate methods for estimation of h-vector from images of crystal projections.[60,61] Singh et al.[56] developed an image-analysis based method to measure h-vector of any crystal using confocal microscopy. Although their method provides direct measurement of h-vector, it requires automation of confocal microscopes for the dynamic measurements of morphology distributions. With further improvements in existing technologies for dynamic measurements the modeling approach presented in the article could provide an effective framework for predictions and control of crystal morphology distributions.

3. MORPHOLOGY DOMAIN: A FUNDAMENTAL PROPERTY OF CRYSTALS

Crystal morphologies are the reflections of the molecular order in crystalline materials. Given the information on crystal structure and the constituting molecules, it is possible to estimate the surface energies using Hartman−Perdok theory (see the discussion in Section 2.2). The low energy surfaces are the F-faces and may be some of the S-faces which are likely to appear during crystal growth. The morphological changes in crystals are due to the appearance or disappearance of faces that can result in a finite number of morphologies. The different morphologies of crystals possible can be obtained from the morphology domain. The morphology domain has some interesting properties that can be exploited for the synthesis of specialized crystals. The subsequent sections will introduce some preliminary concepts toward the establishment of the morphology domain.

3.1. Description of Crystal Morphology. The morphology of a crystal with n number of low energy faces can be represented by a polyhedron, such that

$$\mathbf{Nr} \leq \tilde{\mathbf{h}} \qquad (1)$$

where $\mathbf{N}$ is a matrix formed by stacking, in a single column, the unit normals (the reciprocal lattice vectors) of crystal faces as row vectors, $\mathbf{r}$ represents position vectors in $\mathcal{R}^3$ and $\tilde{\mathbf{h}}$ is a vector of perpendicular distances of faces from the center of the crystal. Therefore, $\tilde{\mathbf{h}}$ is in the non-negative orthant of n-dimensional real space $\mathcal{R}^n_{+0}$. The symmetry of crystals allows the classification of faces into different families. According to crystal growth theories, a family of faces with similar atomic or molecular arrangements grows in an identical manner. However, the dynamics of face transitions are strongly dependent on the shape/geometry of individual faces and constituting neighbors. A crystal can have different shapes of faces forming a family such that there is no synchronization in the face transitions. Further classification based on the shapes of faces in a family would provide groups of kinetically and geometrically similar faces, which in crystallography are referred to as faces of identical *form*. Clearly, the faces of one form will have identical growth rates and they will appear or disappear simultaneously. A crystal with m forms of faces can be represented by m distinct perpendicular distances forming a vector $\mathbf{h} \in \mathcal{R}^m_{+0}$ such that at any time $\tilde{\mathbf{h}}$ can be reconstructed from $\mathbf{h}$. Therefore, the dynamics of crystal morphology can be uniquely determined from $\mathbf{h}$ (*h-vector*).

Example: Potash alum has $n = 26$ low energy faces that can potentially appear during growth. These faces belong to 3 families such as $\{100\}$ containing 6 faces, $\{110\}$ containing 12 faces and $\{111\}$ with 8 faces. In this case all the faces in each family are similar in shape, and therefore the number of families is equal to the number of forms of faces, which is $m = 3$. Conversely, acetaminophen has four families of low-energy faces such as $\{001\}$, $\{011\}$, $\{110\}$, and $\{201\}$ summing up to $n = 14$ faces. Each of these families except $\{201\}$ has two groups of geometrically different faces yielding $m = 7$ forms of faces.

3.2. Morphology Set. As the faces of one form behave in a similar way, their appearances or disappearances completely depend on their growth rates which depend on crystallization conditions. At any time there are only a few forms of faces present on a crystal giving it a unique kind of morphology. Suppose different forms of faces are named as F_1, F_2, ..., F_m whose perpendicular distances from the center of crystal are h_1, h_2, ..., h_m, respectively. The morphology set is a set of all possible types of morphologies obtained from different combinations of F_1, F_2, ..., F_m faces forming a closed polyhedron. The possible combinations of different forms of faces create a power set[62] P containing 2^m subsets of $\{F_1, F_2, ..., F_m\}$ such that

$$P = \{\{F_1, F_2, ..., F_m\}, \{F_2, F_3, ..., F_m\}, ..., \{F_{m-1}, F_m\}, ..., \{F_{m-1}\},$$
$$\{F_m\}, \{\phi\}\}$$

Each set in the power set corresponds to specific forms of faces forming a specific type of polyhedron. According to the definition, the only sets in the power set that form a closed polyhedron will contribute to the morphology set. There exist many theorems for identification of closed convex polyhedron.[63] Euler's formula provides a simpler check for closed polyhedron. A computationally efficient method to identify an open convex polyhedron, without actually constructing it, is

finding a half-space devoid of face-specific normal vectors. Conversely, the absence of such half-spaces will confirm the existence of closed convex polyhedron. Furthermore, the half-spaces can be realized by constructing a convex hull through face-specific unit normals and origin. If the origin lies on/inside the convex hull then the polyhedron is open/closed. Figure 1
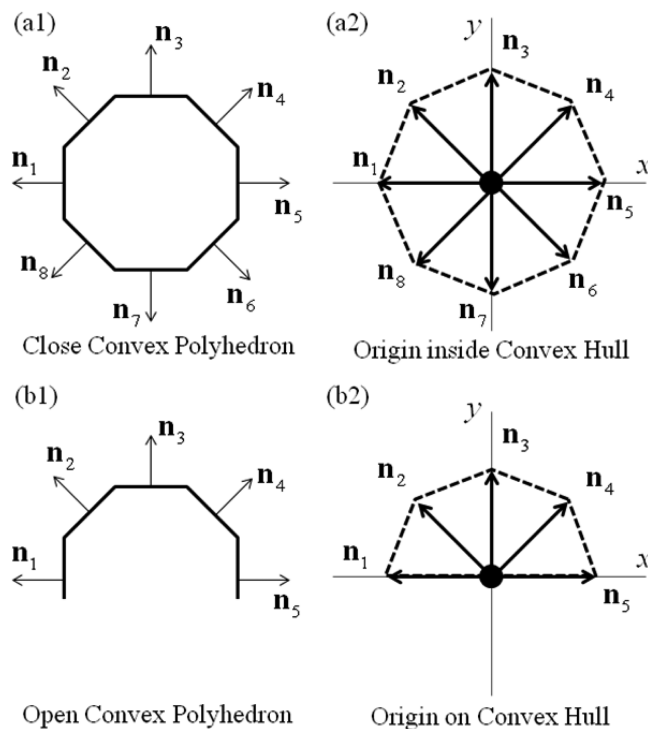
Figure 1. Identification of closed (top row) and opened (bottom row) convex polyhedra. The convex hull (a2) through face normals $\mathbf{n}_i$ of the closed polyhedron (a1) encapsulates the origin, whereas the convex hull (b2) through the normals of the open polyhedron (b1) passes through the origin.

demonstrates the aforementioned technique to identify closed and opened convex polyhedra.

Clearly, the total number of sets in a morphology set will be less than or equal to that of the power set. That means if there are S number of sets in the morphology set then $S \leq 2^m$. The morphology set can be written as $M = \{M_1, M_2, ..., M_S\}$. Every set in the morphology set represents a specific type of morphology that can be described by a fewer number of independent h's corresponding to F's in the set. The faces that are not present in a set are assigned as *virtual* with their h's being dependent on the real faces.
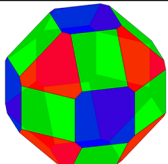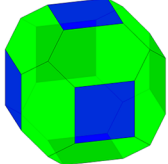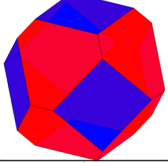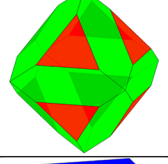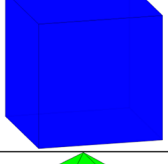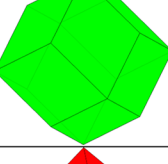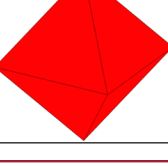
Example: potash alum of the space group $Pa3$ has $m = 3$ forms of faces, namely, $F_1 \equiv \{100\}$, $F_2 \equiv \{110\}$ and $F_3 \equiv \{111\}$. The power set containing $2^3 = 8$ subsets can be written as $P = \{\{F_1,F_2,F_3\}, \{F_1,F_2\}, \{F_1,F_3\}, \{F_2,F_3\}, \{F_1\}, \{F_2\}, \{F_3\}, \{\phi\}\}$. The morphology set of potash alum is constructed from the subsets in power set that form closed polyhedra and is represented as

$$M = \{\{F_1, F_2, F_3\}, \{F_1, F_2\}, \{F_1, F_3\}, \{F_2, F_3\}, \{F_1\}, \{F_2\}, \{F_3\}\}$$
$$= \{M_1, M_2, M_3, M_4, M_5, M_6, M_7\}$$

The total $S = 7$ different morphologies possible for potash alum are listed in Table 1.

3.3. Morphology Graph. Different kinds of morphologies in the morphology set have different sets of real and virtual faces.

Table 1. Morphology Set of Potash Alum with Graphical Representation

| Index Number s	Morphology Set M	Independent h's	Graphical Morphology
1	$M_1 \equiv \{F_1, F_2, F_3\}$	h_1, h_2, h_3	
2	$M_2 \equiv \{F_1, F_2\}$	h_1, h_2	
3	$M_3 \equiv \{F_1, F_3\}$	h_1, h_3	
4	$M_4 \equiv \{F_2, F_3\}$	h_2, h_3	
5	$M_5 \equiv \{F_1\}$	h_1	
6	$M_6 \equiv \{F_2\}$	h_2	
7	$M_7 \equiv \{F_3\}$	h_3	

Some of the real faces of crystal morphology can disappear (become virtual) to produce a different morphology in the morphology set. Likewise, some of the virtual faces of crystal morphology can appear (become real) transforming to a different type of morphology. Two types of morphologies in the morphology set can transform to each other if one is the subset of the other. A morphology graph can be constructed from the morphology set such that every set is connected with its subsets. The morphology graph is a bidirected graph with total R edges and S vertices. The edges are denoted as $e_{s,s'}$, which are connecting the vertices M_s and $M_{s'}$ such that $s < s'$ and $s,s' \in [1, 2, ..., S]$. If there is only one edge connecting two different morphologies (or vertices), then the total number of edges in the morphology graph is given as

$$R = \sum_{i=1}^{S} [2^{\text{card}(M_i)} - 2] \qquad (2)$$

where card(M_i) is the cardinality (measure of a set) of the set M_i. The order of transitions is described as the number of different forms of faces appearing or disappearing simultaneously. It is therefore given as the difference in the cardinality of the connected sets in the morphology graph.

Example: Figure 2 shows the morphology graph of potash alum with $S = 7$ vertices and $R = 14$ edges. In this case $e_{1,5}$, $e_{1,6}$, and $e_{1,7}$ are the second-order transitions because the differences in the cardinalities of connected sets are 2. Similarly, all remaining edges are the first-order transitions. The edge $e_{1,3}$ is composed of three independent edges that relate M_1 to M_3 and is shown in Table 2. That means there are three different ways to attain M_3 from M_1 by the disappearance of F_2 on either (1) F_1, or (2) F_3, or (3) F_1 and F_3.

The dynamics of appearance and disappearance of faces are known as virtual-to-real and real-to-virtual face transitions,
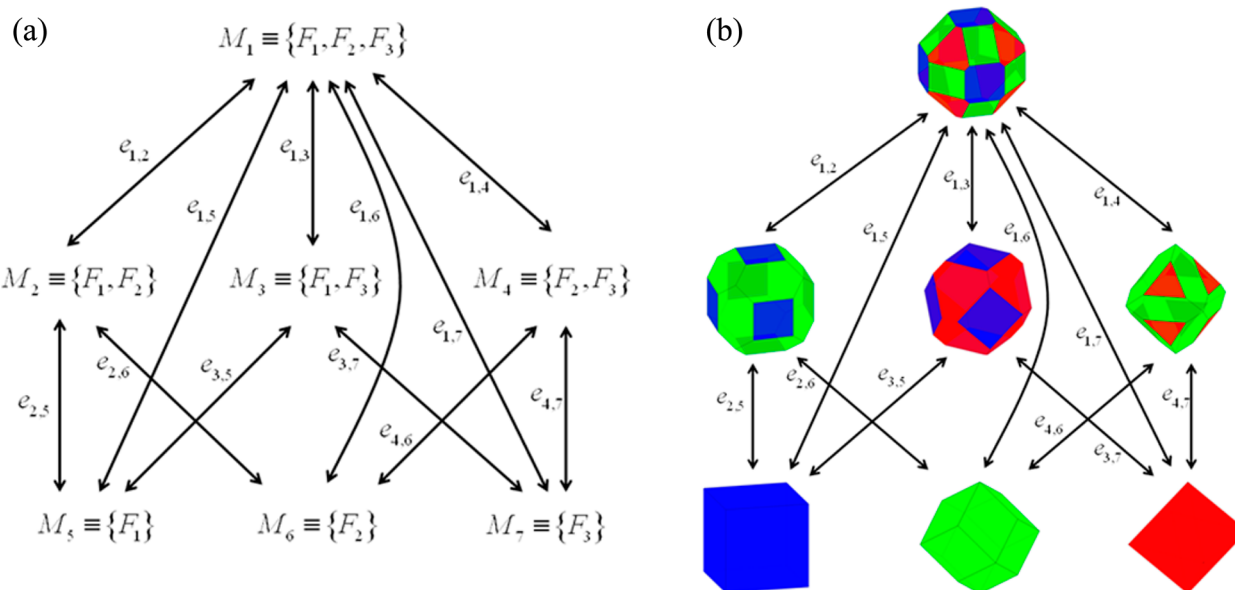
Figure 2. Morphology graph of potash alum. (a) Connected morphology set and (b) connected graphical morphologies.

respectively. Since vertices define edges of a closed convex polyhedron, a face transition can only occur at the vertices. The necessary condition for face transitions is that the neighboring faces must converge to a vertex. The sufficient condition for disappearance of a face is that the real growth rate must be greater than the virtual growth rate of a face and appearance of a face requires its real growth rate to be less than its virtual growth rate. Besides the strict positive values of h's, the necessary conditions provide the upper and lower limit on h with respect to other h's. The necessary condition for the real-to-virtual transition of vth face is given by

$$h_v = \mathbf{n}_v^T \begin{bmatrix} \mathbf{n}_i^T \\ \mathbf{n}_j^T \\ \mathbf{n}_k^T \end{bmatrix}^{-1} \begin{bmatrix} h_i \\ h_j \\ h_k \end{bmatrix} \tag{3}$$

where i,j and k are the indices of faces that are neighbors of the vth face. The necessary condition for the virtual-to-real transition of the vth face is given by

$$h_v < \mathbf{n}_v^T \begin{bmatrix} \mathbf{n}_i^T \\ \mathbf{n}_j^T \\ \mathbf{n}_k^T \end{bmatrix}^{-1} \begin{bmatrix} h_i \\ h_j \\ h_k \end{bmatrix} \tag{4}$$

Equations 3 and 4 provide conditions for first-order face transitions corresponding to each edge in the morphology graph. The higher-order transitions satisfy more than one first-order transitions.

Example: Every edge in the morphology graph corresponds to specific forms of faces undergoing transitions. Table 2 shows the conditions for face transitions for each edge in the morphology graph. The left-hand sides of the conditions contain h's of the faces disappearing and become dependent on those in the right-hand sides. It can be noticed that the h's of disappearing faces become dependent on h's of only a few of the existent faces but not all. These conditions together with

the strict positive values of h-vectors provide bounds on the h-vector.

3.4. Morphology Domain. The edges of morphology graph provide the constraints on the h-vector that confines its domain in $\mathcal{R}_{+0}^m$. Each edge is associated with a set of linear inequalities written as

$$\mathbf{A}_r \mathbf{h} \leq \mathbf{0} \tag{5}$$

where $\mathbf{A}_r$ is a matrix associated with the rth edge. The constraints on the h-vector given by eqs 3 and 4, which in the case of potash alum are the set equations in column 5 and 6 of Table 2, can be written together in matrix notation as

$$\mathbf{A}\mathbf{h} \leq \mathbf{0} \tag{6}$$

which is the equation of a convex polyhedral cone in $\mathcal{R}_{+0}^m$ with vertex at the origin. Here $\mathbf{A} = [\mathbf{A}_r]_{r=1}^R$ is a partitioned matrix formed by column-wise stacking of $\mathbf{A}_r$. Clearly, the row vectors of $\mathbf{A}$ are the face-specific normals of polyhedral cone. The morphology domain is defined as the phase space of crystal morphologies confined in the polyhedral cone in $\mathcal{R}_{+0}^m$ and is described as

$$C = \{\mathbf{h} \in \mathcal{R}_{+0}^m | \mathbf{A}\mathbf{h} \leq \mathbf{0}\} \tag{7}$$

Any point in the interior of the morphology domain represents a crystal of specific size and morphology. The $\mathbf{h}$ corresponding to the point can be converted to $\tilde{\mathbf{h}}$ which when supplied to eq 1 will give the crystal morphology. The morphology domain is the fundamental property of crystals that yields phase diagrams showing regions of different morphologies. The morphology domain has the following important attributes:

(1) If the faces that are likely to be present on a crystal are the low-energy faces, then the resulting morphology domain will give all possible morphologies of the crystal. The morphology domain is only dependent on the crystal structure and is independent of crystallization conditions.

(2) Broader the morphology domain, the wider would be the collection of crystal morphologies. And the narrower domain will allow only a few morphologies of crystals.

Table 2. Edge-Specific Conditions for Face Transitions in Potash Alum

Edge Number	Edge Name	Order of Transition	Faces Undergoing Transitions	Conditions for Disappearances	Conditions for Appearances
1	$e_{1,2}$	First	F_3	$h_3 = \frac{\sqrt{3}}{\sqrt{2}} h_2$	$h_3 < \frac{\sqrt{3}}{\sqrt{2}} h_2$
2	$e_{1,3(1)}$	First	F_2	$h_2 = \sqrt{2} h_1$	$h_2 < \sqrt{2} h_1$
3	$e_{1,3(2)}$	First	F_2	$h_2 = \frac{\sqrt{3}}{\sqrt{2}} h_3$	$h_2 < \frac{\sqrt{3}}{\sqrt{2}} h_3$
4	$e_{1,3(3)}$	First	F_2	$h_2 = \sqrt{2} h_1, h_2 = \frac{\sqrt{3}}{\sqrt{2}} h_3$	$h_2 < \sqrt{2} h_1, h_2 < \frac{\sqrt{3}}{\sqrt{2}} h_3$
5	$e_{1,4}$	First	F_1	$h_1 = \sqrt{2} h_2$	$h_1 < \sqrt{2} h_2$
6	$e_{2,5}$	First	F_2	$h_2 = \sqrt{2} h_1$	$h_2 < \sqrt{2} h_1$
7	$e_{2,6}$	First	F_1	$h_1 = \sqrt{2} h_2$	$h_1 < \sqrt{2} h_2$
8	$e_{3,5}$	First	F_3	$h_3 = \sqrt{3} h_1$	$h_3 < \sqrt{3} h_1$
9	$e_{3,7}$	First	F_1	$h_1 = \sqrt{3} h_3$	$h_1 < \sqrt{3} h_3$
10	$e_{4,6}$	First	F_3	$h_3 = \frac{\sqrt{3}}{\sqrt{2}} h_2$	$h_3 < \frac{\sqrt{3}}{\sqrt{2}} h_2$
11	$e_{4,7}$	First	F_2	$h_2 = \frac{\sqrt{3}}{\sqrt{2}} h_3$	$h_2 < \frac{\sqrt{3}}{\sqrt{2}} h_3$
12	$e_{1,5}$	Second	F_2, F_3	$h_2 = \sqrt{2} h_1, h_3 = \sqrt{3} h_1$	$h_2 < \sqrt{2} h_1, h_3 < \sqrt{3} h_1$
13	$e_{1,6}$	Second	F_1, F_3	$h_1 = \sqrt{2} h_2, h_3 = \frac{\sqrt{3}}{\sqrt{2}} h_2$	$h_1 < \sqrt{2} h_2, h_3 < \frac{\sqrt{3}}{\sqrt{2}} h_2$
14	$e_{1,7}$	Second	F_1, F_2	$h_1 = \sqrt{3} h_3, h_2 = \frac{\sqrt{3}}{\sqrt{2}} h_3$	$h_1 < \sqrt{3} h_3, h_2 < \frac{\sqrt{3}}{\sqrt{2}} h_3$

(3) The polyhedral symmetry of the crystals decreases as moving away from the space diagonal. Therefore, the most symmetric crystals lie on the space diagonal.

These interesting properties of morphology domain help in identifying the target morphologies of crystals based on the different applications. For example, (i) pharmaceuticals require more symmetric crystals for ease in downstream processing, (ii) tuning the band gap energies of semiconductor particles require selection of specific shapes such as spheres, rods, or plates, and (iii) better activities of catalyst particles require larger fraction of reactive faces. The targeting of crystal morphologies can be readily done using the morphology domain. However, the attainability of such targets requires the dynamic studies of crystal morphologies inside morphology domain, which will be discussed in the subsequent section.
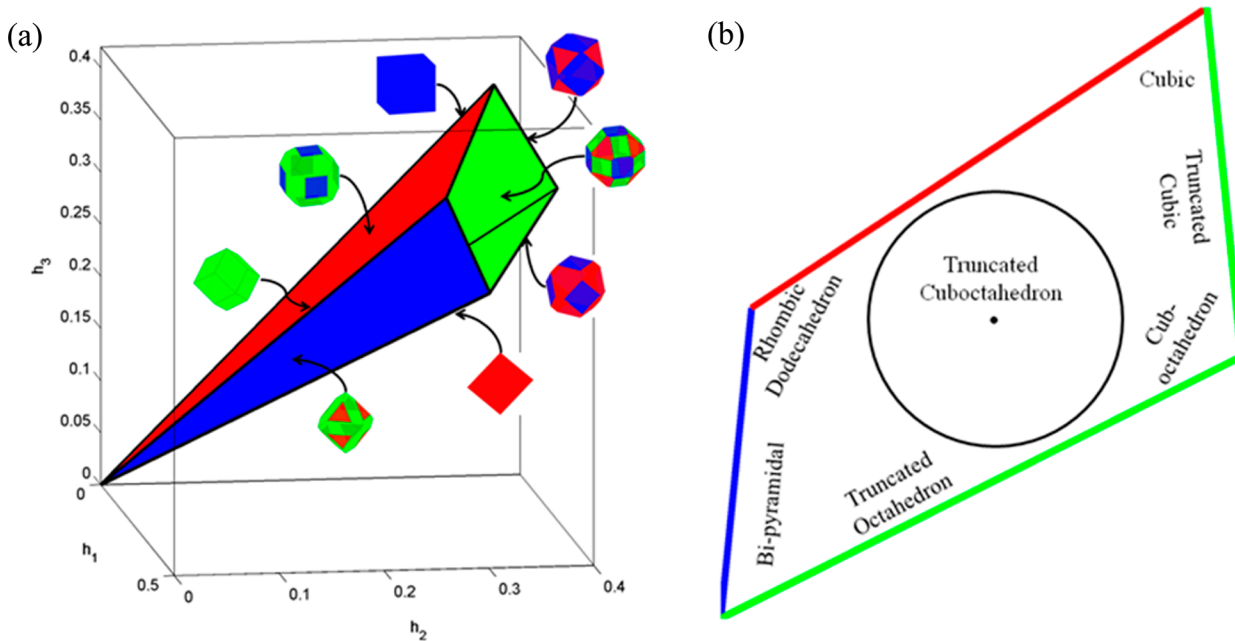
Example: The morphology domain of potash alum, given by the set of equations in Table 2 or eq 6, is shown graphically in Figure 3a. Although there are 14 edges in the morphology graph, the number of faces in the morphology domain is 4, which means that the remaining 10 planes are either on the edges of the morphology domain or they are repeated. The faces, edges, and interior of the morphology domain represent domains of different morphologies.

The domains of different morphologies in the morphology domain are identified as M_1- interior, M_2- red plane, M_3- green planes, M_4- blue plane, M_5- intersection of red and green planes, M_6- intersection of red and blue planes, and M_7- intersection of blue and green planes. Unlike all other domains, M_3 is a hybrid domain formed by two planes and one edge. The cross section of the morphology domain along the (111) direction, shown in Figure 3b, identifies different regions of Archimedean shapes that potash alum can take. Interestingly, potash alum can only grow in symmetric shapes and cannot take shapes such as needles and plates, which is a constraint imposed by its crystal structure.

4. SINGLE CRYSTAL MODEL

The dynamics of crystal morphologies are governed by the face-specific growth rates that can be determined from either experiments or theory (discussed in Section 2.2). The face-specific growth rates are expressed as m dimensional vector $\dot{\mathbf{H}}(\mathbf{h}, \mathbf{c})$, which can be a function of h-vector and crystallization conditions. Since $\dot{\mathbf{H}}(\mathbf{h}, \mathbf{c})$ represents growth rates of real faces, it can take different values if some of the faces disappear (or becoming virtual). Each kind of morphology in the morphology set has an associated set of real and virtual faces (see Table 2). The growth rates of virtual faces are dependent on the real faces which can be realized by taking time derivatives of eq 3. Therefore, there exists a unique growth rate vector for each type of morphology in the morphology set. The projection matrix $\mathbf{P}_s$ can be defined such that the modified growth rate vector for morphology in the sth domain is given as $\mathbf{P}_s(\dot{\mathbf{H}})\dot{\mathbf{H}}(\mathbf{h}, \mathbf{c})$.

Figure 3. (a) Morphology domain of potash alum and (b) cross section of the morphology domain along (111) plane indicating regions of different Archimedean solids.

The projection matrix is a continuous function of $\dot{\mathbf{H}}$ and varies discretely with domains.

The morphology domain is the direct sum or union of the domains of individual morphologies, such that

$$C = C_1 + C_2 + \dots + C_S \tag{8}$$

where C_s are the domains (generalized polyhedral cones) corresponding to the morphologies M_s in the morphology domain C and they are identified as

$$C_s = \{\mathbf{h} \in C | \mathbf{A}_r \mathbf{h} = \mathbf{0}, \; e_{s,s,} = e_{1,s}\}, \; s \in [2, 3, \dots, S] \tag{9}$$

Equation 9 says that equalities $\mathbf{A}_r \mathbf{h} = \mathbf{0}$ associated with the edges $e_{1,s}$ which are originating from M_1 and leading to M_s will define the domain C_s. Henceforth, the equalities associated with the specific edges $e_{1,s}$ will be denoted as $\mathbf{D}_s \mathbf{h} = \mathbf{0}$. The generalized architecture of morphology domain is such that every other domain $C_2, C_3, \dots, C_S$ is connected with C_1 (the interior of the morphology domain), where

$$C_1 = \{\mathbf{h} \in C | \mathbf{A}\mathbf{h} < \mathbf{0}\} \tag{10}$$

The dynamic equation for the evolution of single crystal morphology can now be expressed as

$$\frac{d\mathbf{h}}{dt} = \alpha_s(\dot{\mathbf{H}})\mathbf{P}_s(\dot{\mathbf{H}})\dot{\mathbf{H}}(\mathbf{h}, \mathbf{c}), \; \mathbf{h} \in C_s \tag{11}$$

The prefactor $\alpha_s(\dot{\mathbf{H}})$ scales the projected growth rate vector $\mathbf{P}_s\dot{\mathbf{H}}$ such that the real growth rates are unaltered. As mentioned before the projection matrix is not a continuous function of $\mathbf{h}$ and changes discretely with different domains of morphology within the morphology domain, such that

$$\mathbf{P}_s(\dot{\mathbf{H}}) = \sum_i \boldsymbol{\nu}_i \boldsymbol{\nu}_i^T + \sum_j \boldsymbol{\mu}_j \boldsymbol{\mu}_j^T, \; \boldsymbol{\nu}_i \in N(\mathbf{D}_s) \text{ and } \boldsymbol{\mu}_j \in N(\mathbf{G}_s) \tag{12}$$

where $\boldsymbol{\nu}_i$ and $\boldsymbol{\mu}_j$ are the orthonormal basis vectors of the null-space of the matrix $\mathbf{D}_s$ and $\mathbf{G}_s$, respectively. Here, the matrix $\mathbf{D}_s$ corresponds to the lowest possible domain s for which

$\mathbf{D}_s \mathbf{h} = \mathbf{0}$ and $\mathbf{D}_s \dot{\mathbf{H}} \geq \mathbf{0}$. Any domain has a set of real faces and virtual faces (see Table 2), the growth rate of virtual faces are related as $\mathbf{D}_s \dot{\mathbf{H}} = \mathbf{0}$, and the growth rates of real faces can be expressed as a symmetric equation of line, $\mathbf{G}_s \dot{\mathbf{H}} = \mathbf{0}$. The matrix $\mathbf{G}_s$ is a bidiagonal matrix with the number of rows being one less than the number of real faces (F) present on the crystal. If there are no virtual faces (first domain) then the projection matrix is the identity matrix.

$$\mathbf{P}_1(\dot{\mathbf{H}}) = \mathbf{I} \tag{13}$$

Consider a crystal growing by surface-integration under fixed crystallization conditions such that $\dot{\mathbf{H}}$ is constant. If we know the initial condition for $\mathbf{h}$ then the projection matrix $\mathbf{P}_s(\dot{\mathbf{H}})$ and the prefactor are also fixed. The solution of eq 11 can be written as $\mathbf{h}(t) = \mathbf{h}(0) + \alpha_s \mathbf{P}_s \dot{\mathbf{H}} t$ which at suitably longer time scales gives the condition for steady-state morphology.

$$\mathbf{h} \propto \alpha_s \mathbf{P}_s \dot{\mathbf{H}} \tag{14}$$

The effect of initial condition diminishes over time, and all crystals unanimously converge to the single steady-state morphology, which can be observed in Figure 4.

5. MORPHOLOGICAL-POPULATION BALANCE MODEL (M-PBM)

In this section, we will develop dynamic equations for morphology distributions of crystal populations growing in a batch crystallizer. The morphology distribution is described by a number density $n(\mathbf{h}, t)$ of crystals in the morphology domain. The population dynamics in different domains are driven by different growth fields $\alpha_s \mathbf{P}_s \dot{\mathbf{H}}$.

The dynamics of morphology distributions in each domain are described by population balance equations. The change in morphology distribution in the sth domain is due to two primary factors: (i) growth field $\alpha_s \mathbf{P}_s \dot{\mathbf{H}}$ and (ii) feed $\dot{B}_s$ coming to sth domain from other connected domains. As the crystals growing-out and leaving the sth domain cannot affect the morphology distribution of its own domain, this effect is not
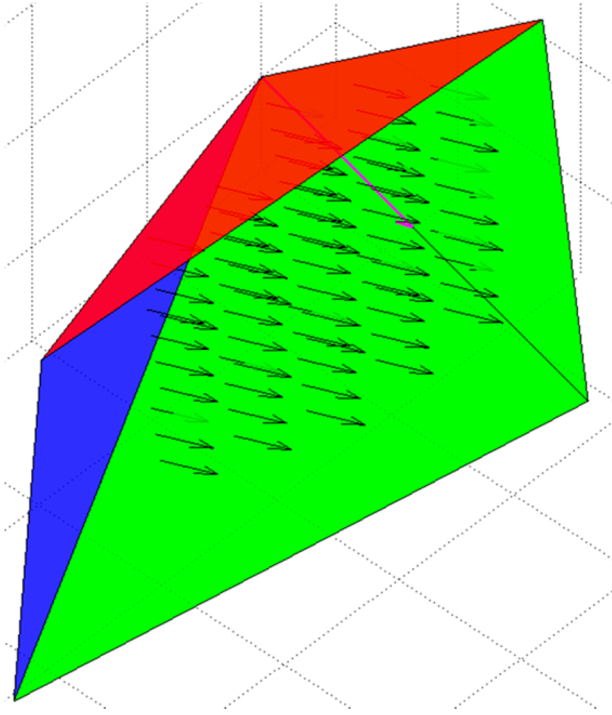
Figure 4. Different crystals of potash alum growing (black arrows) in an identical growth field and converging to a steady-state morphology (magenta arrow).

considered in formulating population balance equations. The projection matrix $\mathbf{P}_s$ specific to sth domain can be obtained from the matrices $\mathbf{D}_s$ and $\mathbf{G}_s$. For the sake of brevity, we will use $\mathbf{P}_s$ for the combined expression $\alpha_s \mathbf{P}_s$ which can be referred to as scaled-projection matrix.

The feed from other domains can come to the sth domain if they are directly connected with it. The connectivity of the domains can be elucidated from the morphology graph. Here, we consider an analogous morphology graph with first-order transitions where edges are connecting a set to its subset in a forward direction. The vertices and edges of this unidirected morphology graph are related using incidence matrix $\mathbf{G} = [g_{s,r}]$ as

$$\mathbf{M} = \mathbf{GE} \tag{15}$$

where $\mathbf{M} = [M_s]$ is an $S \times 1$ vector of vertices and $\mathbf{E} = [e_{s,s'}]$ is a column vector of first-order edges. The positive elements in the row vector of $\mathbf{G}$ indicate feed coming from higher domains, and the negative elements indicate feed coming from lower domains. The set of first-order edges that may feed the sth domain from the higher domains can be identified as

$$J_s^+ = \{r \in [1, 2, ..., R] | g_{s,r} = +1, \mathbf{D}_s\dot{\mathbf{H}} > 0\}, \ s \in [1, 2, ..., S] \tag{16}$$

And the set of first-order edges that will feed the sth domain from the lower domains is given as

$$J_s^- = \{r \in [1, 2, ..., R] | g_{s,r} = -1, \mathbf{D}_s\dot{\mathbf{H}} < 0\}, \ s \in [1, 2, ..., S] \tag{17}$$

The information from J_s^+ and J_s^- can used together to generate flux maps, which depend on the growth rate vectors. Now, generalized population balance equations can be formulated in a domain C_s considering the fluxes coming from higher domains.

$$\frac{\partial}{\partial t}n(\mathbf{h}, t) + \nabla \cdot \mathbf{P}_s\dot{\mathbf{H}}(\mathbf{h}, \mathbf{c})n(\mathbf{h}, t) = \dot{B}_s, \ \mathbf{h} \in C_s \tag{18}$$

The feed rate $\dot{B}_1$ for C_1 is zero because it is the highest domain in the morphology domain. The population balance equation for C_1 is given as

$$\frac{\partial}{\partial t}n(\mathbf{h}, t) + \nabla \cdot \dot{\mathbf{H}}(\mathbf{h}, \mathbf{c})n(\mathbf{h}, t) = 0, \ \mathbf{h} \in C_1 \text{ and } \mathbf{A}\dot{\mathbf{H}} < \mathbf{0} \tag{19}$$

The structure of $\dot{B}_s$ is determined by J_s^+ which accounts for the fluxes coming from higher domains and it can be written as

$$\dot{B}_s = \sum_{r \in J_s^+} \mathbf{A}_r\mathbf{P}_s\dot{\mathbf{H}}\delta(\mathbf{A}_r\mathbf{h})n(\mathbf{h}, t)|_{\mathbf{D}_r\mathbf{h}=0} \atop {\mathbf{A}_r\mathbf{h}=0^-} \tag{20}$$

It can be seen that $\dot{B}_s$ only accounts for first-order transitions. The fluxes due to higher-order transitions are already accounted as a linear combination of first-order transitions in eq 20. There are some additional equations accounting for fluxes coming from lower domains, which are given as

$$\mathbf{P}_s\dot{\mathbf{H}}n(\mathbf{h}, t)|_{\mathbf{D}_s\mathbf{h}=0} = \mathbf{P}_r\dot{\mathbf{H}}n(\mathbf{h}, t)|_{\mathbf{D}_r\mathbf{h}=0}, \ r \in J_s^- \atop {\mathbf{A}_r\mathbf{h}=0^-} \tag{21}$$

The morphological-population balance eqs 18 and 19 are subjected to the following boundary conditions.

$$\|\mathbf{P}_s\dot{\mathbf{H}}(\mathbf{0}, \mathbf{c})\| n(\mathbf{0}, t) = 0 \tag{22}$$

$$\mathbf{P}_s\dot{\mathbf{H}}(\mathbf{h}, \mathbf{c})n(\mathbf{h}, t) \to \mathbf{0}, \ \|\mathbf{h}\| \to \infty \tag{23}$$

The right-hand side of eq 22 can take a nonzero quantity in presence of nucleation. The boundary condition (23) is often referred to as a *regularity condition*.

The growth of crystal populations consumes supersaturation, which again affects face-specific growth rates. The dynamics of supersaturation in a batch crystallizer coupled with the number density, such that

$$S(t) = \frac{c_0 - \rho \int_c [n(\mathbf{h}, t) - n(\mathbf{h}, 0)] \, d\mathbf{h}}{c_{sat}} \tag{24}$$

where c_0 is the initial concentration, c_{sat} is the saturation concentration, ρ is the crystal density, and S is the supersaturation which is defined as ratio of bulk concentration to saturation concentration. As growth rates are a function of supersaturation, dynamic analysis of morphology distributions with population balances must take into account the reciprocal effects of the crystal growth on supersaturation.

Thus, eqs 18, 19, 21, and 24 form a morphological-population balance model for crystal morphology distributions whose solution will be discussed in Section 6. The morphological-population balance model (M-PBM) for potash alum is developed in Appendix I. The consistency of M-PBM can be checked by number balance.

6. SOLUTION OF M-PBM

The morphological-population balance equations are a set of hyperbolic partial differential equations, whose solution can be obtained using the method of characteristics.[64] The characteristic of eq 18 is given by eq 11. Evolution of the number density along the characteristic can be written as

$$\frac{d}{dt}n(\mathbf{h}, t) = \dot{B}_s, \ \mathbf{h} \in C_s \tag{25}$$
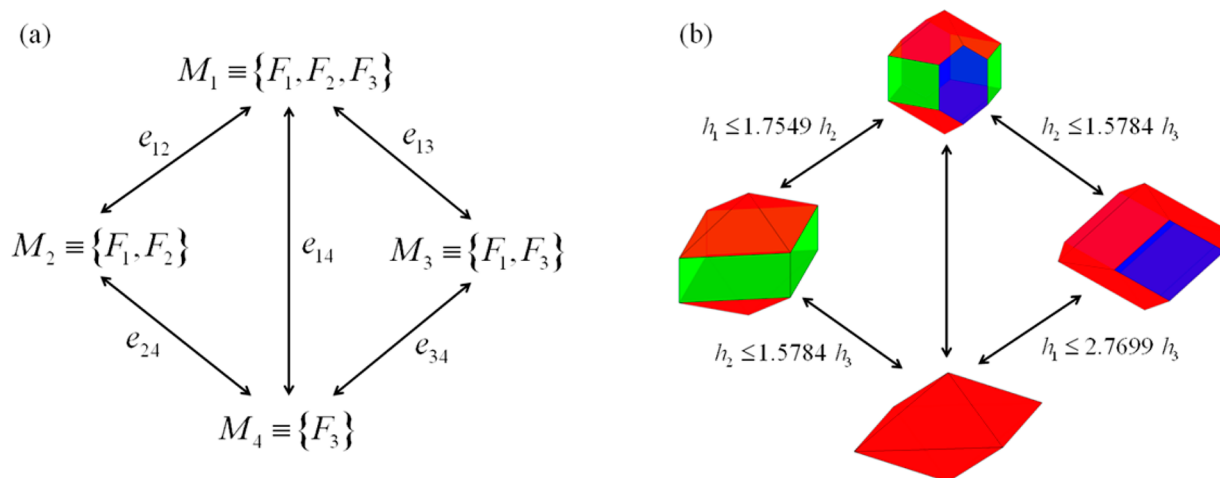
Figure 5. Morphology graph of KAP.[40] (a) Connected morphology set and (b) connected graphical morphologies with edges showing conditions for face transitions.
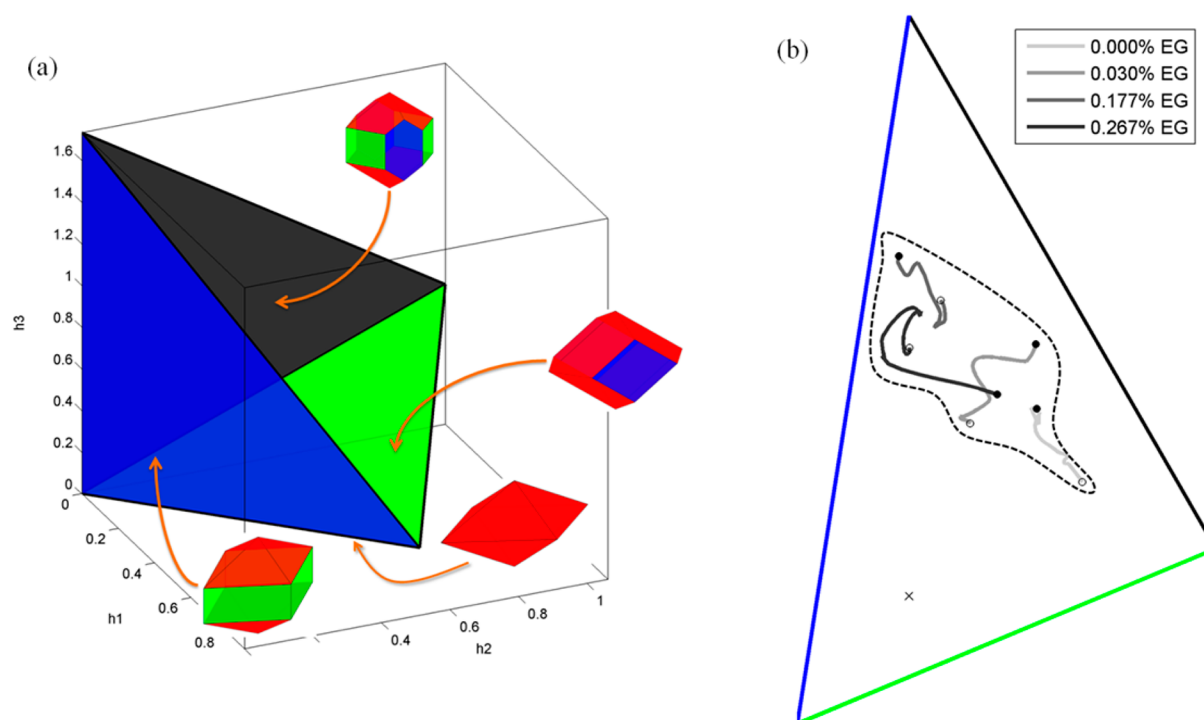

Figure 6. (a) Morphology domain of KAP and (b) cross section of the morphology domain along the (111) direction showing region of steady-state morphologies (dashed line). Each line in that region represents the trajectory of steady-state morphology at fixed concentration of ethylene glycol (EG) and varying supersaturation from 1% (dark circle) to 5% (open circle).

Since the feed rate $\dot{B}_s$ is independent of number density in C_s, the solution of eq 25 can be obtained as

$$n(\mathbf{h}, t) = n(\mathbf{h}, 0) + \int_0^t \dot{B}_s(t') \, \mathrm{d}t', \quad \mathbf{h} \in C_s \tag{26}$$

The solutions for number densities obtained by time integration in eq 26 are mutually coupled with the mass balance equation (eq 24) through the characteristics.

7. ADDITIVE CONTROLLED CRYSTALLIZATION OF POTASSIUM HYDROGEN PHTHALATE

Potassium hydrogen phthalate ($C_8H_5O_4K$, KHP, or KAP) crystals are the molecular ionic solids that are used as buffering agents, standards for total organic carbon testing, monochromators and

analysers in X-ray diffractometers and many other applications. The connected net analysis of KAP yielded three relatively energetic F-faces such as {010}, {110}, and {111} that are more likely to appear during crystal growth. The morphology graph and morphology domain are already established for KAP.[40] The morphology graph of KAP is shown in Figure 5 which connects the four different morphologies through four edges.

The morphology domain of KAP can be constructed using conditions of face transitions shown in Figure 5b. Figure 6a shows the morphology domain of KAP, and Figure 6b shows the cross section of the morphology domain along the (111) direction. The broader morphology domain of KAP can accommodate a wider range of morphologies than potash alum. The accessible morphologies in the morphology domain are governed by the

growth rates. Kuznetsov et al.[65] experimentally measured the growth rates of KAP at different supersaturations and concentrations of ethylene glycol (an additive). Steady-state morphologies of KAP at different supersaturations and concentrations of ethylene glycol can be obtained from eq 14, and the region spanned is shown in Figure 6b.

The region of steady-state morphologies also indicates the directions of growth rate vector $\dot{\mathbf{H}}(\sigma, x_{EG})$. Here, the growth rates are a function of relative supersaturation $\sigma = (S - 1)\%$ and mole percent x_{EG} of ethylene glycol in the aqueous solution of KAP. The growth rate vectors are confined in the morphology domain such that $\mathbf{A}\dot{\mathbf{H}} < 0$. The flux map resulting from the growth rate vectors is shown in Figure 7.
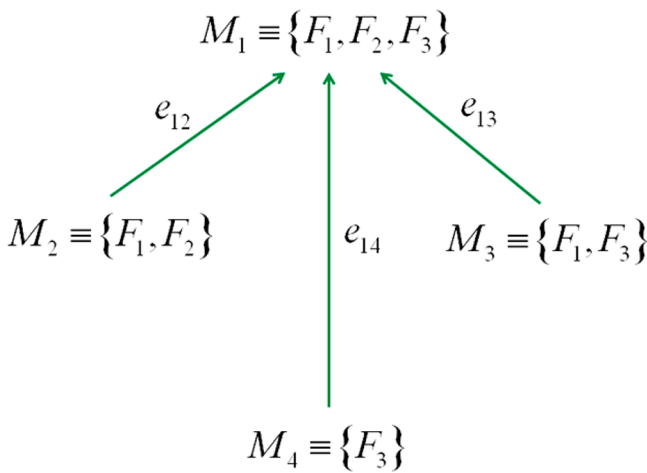
Figure 7. Flux of map of KAP crystals growing in the aqueous solution containing ethylene glycol additive.

Consider a population of seed crystals of morphology M_1 growing in a batch crystallizer. The governing population balance equation corresponding to the flux map in Figure 7 can be written as

$$\frac{\partial}{\partial t} n(\mathbf{h}, t) + \dot{\mathbf{H}}(\sigma, x_{EG}) \nabla n(\mathbf{h}, t) = 0, \quad \mathbf{h} \in C_1 \qquad (27)$$

Since the crystals of other morphologies are not present, there will be no influx of crystals from lower domain. The solution of eq 27 along the characteristics

$$\frac{d\mathbf{h}}{dt} = \dot{\mathbf{H}}(\sigma, x_{EG}) \qquad (28)$$

is given as

$$n(\mathbf{h}, t) = n(\mathbf{h}(t), 0) \qquad (29)$$

The evolution of supersaturation is then given by eq 24 and the mole percent of ethylene glycol is related to supersaturation as

$$x_{EG}(t) = \frac{c_{EG}}{\left(\frac{\sigma(t)}{100} + 1\right) c_{sat}(T)} \times 100 \qquad (30)$$

7.1. Additive Controlled Crystallization. Consider the cooling batch crystallization of KAP from aqueous solution using ethylene glycol as additive. Usually, the manufacturing targets in such systems are high productivity and better product quality such as sphericity and purity of crystals. Seeded crystallization under moderate supersaturation is mostly preferred in large scale synthesis to minimize nucleation. If the seed crystals (pre-

Table 3. Parameters and Initial Conditions for KAP Crystallization

parameter	value
density of KAP: ρ	1640 kg/m^3
saturation concentration: $c_{sat}(T)$	$0.032T^2(K) - 16.1742T(K) + 2091.2$ kg/m^3
initial conditions	value
initial concentration of KAP: c_0	153.01 kg/m^3
number of seed crystals: N	1×10^{11} m^{-3}
initial seed distribution	Gaussian distribution
mean $E\mathbf{h}$	$[0.5\ 0.5\ 5]^T$ μm
variance $V\mathbf{h}$	$[2.5\ 2.5\ 5.5]^T \times 10^{-3}$ μm^2
material domain of seed distribution	$Eh_i - 2(Vh_i)^{1/2} \leq h_i \leq Eh_i + 2(Vh_i)^{1/2}$, $i = 1, 2, 3$
initial volume fraction of seed	1.0766×10^{-6}
initial mass of seed crystals	1.8×10^{-3} kg/m^3
average sphericity	0.5291

nucleated) are needle shaped then synthesizing crystals, without sacrificing their productivity, of better sphericity requires proper tuning of operating conditions such as temperature and additive concentration. The optimization problem can now be stated as follows: Maximize the sum of mass fraction and sphericity of crystals growing in a batch crystallizer for 100 s by manipulating temperature and additive concentration. The parameters and initial conditions for the problem are given in Table 3.

The optimization problem maximizes final sphericity to 0.7681 and final mass to 0.8187 kg/m^3 for $\sigma = 5\%$ and $x_{EG} = 0.03$ mol %. The necessary temperature and ethylene glycol concentration to maintain the required σ and x_{EG} are 308 K and 22.4 mM, respectively. The final mean size and shape of the crystals are given by $E\mathbf{h} = [4.51\ 7.34\ 14.71]^T$ μm. The mean aspect ratio of crystals is reduced from 10 to 3, which is a 70% reduction.

The analysis of morphology distributions among crystal populations was restricted to cases without the phenomenon of nucleation. Inclusion of nucleation would require the added arsenal of nucleation kinetics with information on morphology distribution of freshly formed nuclei.

8. CONCLUSIONS

This article presents a generalized framework for dynamics of single crystal morphology and morphology distributions. The systematic approach to identify dynamic equations can be summarized as follows:

Step 1: Determine low-energy faces (F-faces) of a crystalline material using Hartman−Perdok theory and group them according to kinetic and geometric similarity (forms) of faces.

Step 2: Identify morphology set, morphology graph, and morphology domain for a crystal. They can be readily identified using software *MorphologyDomain*.[41] The matrices A_r and D_s will be determined in this step.

Step 3: Obtain the growth rate vector $\dot{\mathbf{H}}$ and identify prefactor α_s and projection matrices P_s for each domain. The evolution of single crystal morphology can now be described by eq 11.

Step 4: Develop an analogous morphology graph with first-order edges and determine the corresponding incidence matrix G. Identify the set of edges J_s^+ connecting the higher domains and the set J_s^- connecting the lower domains with the sth domain, respectively. The flux maps can be created using J_s^+ and J_s^-.

Step 5: The M-PBM can now be developed from eqs 18, 19, 21, and 24. The solution of M-PBM can be obtained by the method of characteristics.

The M-PBM and single crystal model describe dynamics of crystal morphology due to crystal growth in morphology domain. The effect of other processes such as nucleation, breakage, and agglomeration on morphology distributions can be incorporated in M-PBM following the identification of appropriate kernels. For example, the nucleation kernels can be determined from the Gibbs critical nucleation theory where crystal nuclei take equilibrium morphologies. The formulation of breakage kernels require the identification of cleavage planes which determine the likely faces to appear during breakage. Accounting for agglomeration introduces considerable additional complexity. Thus the framework developed here is applicable for relatively lean population densities of crystals.

The morphology domain is a material property of crystals that is independent of crystallization conditions, although trajectories of growing or dissolving crystals in the former depend on the latter. The morphology domain can be considered as a phase diagram for crystalline materials, which presents all possible morphologies of a crystal. Morphology domain can also help in discovering crystal morphologies that are possible but have yet to be found experimentally.

The solution of M-PBM can be quickly obtained from the method of characteristics which enables it for model-based control of crystal morphologies. Obviously, such solutions are also amenable to use in conjunction with other methods for morphology domain due to Borchert et al.[39] The methodology was implemented for additive-controlled crystallization of KAP. The M-PBM of KAP and its solution was discussed in Section 7. The needle-like crystals of KAP was modified to more symmetric crystals by controlling temperature and additive concentration. The current framework provides a great opportunity for discovery of new crystal morphologies and platform for efficient model-based control.

■ APPENDIX I: M-PBM FOR POTASH ALUM

The formulation of M-PBM requires identification of morphology set, morphology graph, $\mathbf{A}_r$ (morphology domain), $\mathbf{D}_s$, $\mathbf{P}_s$, $\mathbf{G}$, J_s^+, J_s^-, and $\dot{B}_s$. The morphology set, morphology graph, and $\mathbf{A}_r$ for potash alum are shown in Table 1, Figure 2, and Table 2 respectively. A user-friendly software called morphology domain[41] can synthesis the morphology set,
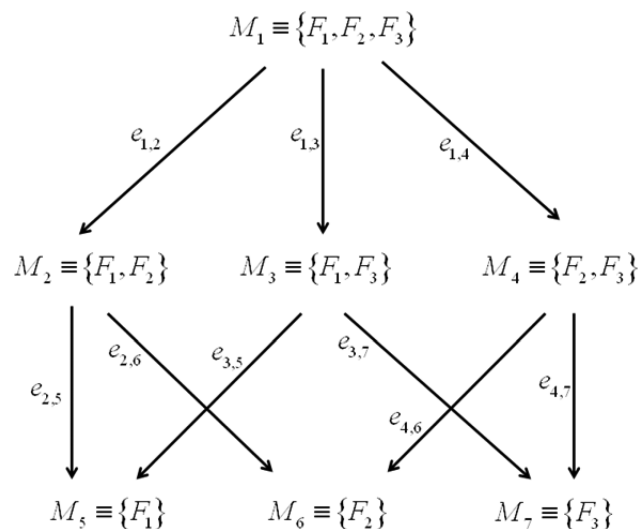

Figure A1. Morphology graph of potash alum with first-order transition in the forward direction.

Table A1. Values of $\mathbf{D}_s$, $\mathbf{G}_s$, α_s, and $\mathbf{P}_s$ for Fixed Growth Rate Vector $\dot{\mathbf{H}} \equiv \begin{bmatrix} \dot{H}_1 & \dot{H}_2 & \dot{H}_3 \end{bmatrix}^T = \begin{bmatrix} 1 & 1.5 & 1.8 \end{bmatrix}^T$ of Potash Alum

s	$\mathbf{D}_s$	$\mathbf{G}_s$	α_s	$\mathbf{P}_s$
1	–	$\begin{bmatrix} \dot{H}_2 & -\dot{H}_1 & 0 \\ 0 & \dot{H}_3 & -\dot{H}_2 \end{bmatrix}$	1	$\begin{bmatrix} 1.0000 & 0.0000 & 0.0000 \\ 0.0000 & 1.0000 & 0.0000 \\ 0.0000 & 0.0000 & 1.0000 \end{bmatrix}$
2	$\begin{bmatrix} 0 & -\dfrac{\sqrt{3}}{\sqrt{2}} & 1 \end{bmatrix}$	$\begin{bmatrix} \dot{H}_2 & -\dot{H}_1 & 0 \end{bmatrix}$	1.0104	$\begin{bmatrix} 0.1509 & 0.2264 & 0.2773 \\ 0.2264 & 0.3396 & 0.4160 \\ 0.2773 & 0.4160 & 0.5094 \end{bmatrix}$
3(1)	$\begin{bmatrix} -\sqrt{2} & 1 & 0 \end{bmatrix}$	$\begin{bmatrix} \dot{H}_3 & 0 & -\dot{H}_1 \end{bmatrix}$	0.9810	$\begin{bmatrix} 0.1603 & 0.2266 & 0.2885 \\ 0.2266 & 0.3205 & 0.4079 \\ 0.2885 & 0.4079 & 0.5192 \end{bmatrix}$
3(2)	$\begin{bmatrix} 0 & 1 & -\dfrac{\sqrt{3}}{\sqrt{2}} \end{bmatrix}$	$\begin{bmatrix} \dot{H}_3 & 0 & -\dot{H}_1 \end{bmatrix}$	1.2058	$\begin{bmatrix} 0.1099 & 0.2423 & 0.1978 \\ 0.2423 & 0.5341 & 0.4361 \\ 0.1978 & 0.4361 & 0.3560 \end{bmatrix}$
3(3)	$\begin{bmatrix} -\sqrt{2} & 1 & 0 \\ 0 & 1 & -\dfrac{\sqrt{3}}{\sqrt{2}} \end{bmatrix}$	–	0.8334	$\begin{bmatrix} 0.2308 & 0.3264 & 0.2665 \\ 0.3264 & 0.4615 & 0.3768 \\ 0.2665 & 0.3768 & 0.3077 \end{bmatrix}$
4	$\begin{bmatrix} 1 & -\sqrt{2} & 0 \end{bmatrix}$	$\begin{bmatrix} 0 & \dot{H}_3 & -\dot{H}_2 \end{bmatrix}$	1.3126	$\begin{bmatrix} 0.4505 & 0.3185 & 0.3822 \\ 0.3185 & 0.2252 & 0.2703 \\ 0.3822 & 0.2703 & 0.3243 \end{bmatrix}$
5	$\begin{bmatrix} -\sqrt{2} & 1 & 0 \\ -\sqrt{3} & 0 & 1 \end{bmatrix}$	–	0.9617	$\begin{bmatrix} 0.1667 & 0.2357 & 0.2887 \\ 0.2357 & 0.3333 & 0.4082 \\ 0.2887 & 0.4082 & 0.5000 \end{bmatrix}$
6	$\begin{bmatrix} 1 & -\sqrt{2} & 0 \\ 0 & -\dfrac{\sqrt{3}}{\sqrt{2}} & 1 \end{bmatrix}$	–	1.3187	$\begin{bmatrix} 0.4444 & 0.3143 & 0.3849 \\ 0.3143 & 0.2222 & 0.2722 \\ 0.3849 & 0.2722 & 0.3333 \end{bmatrix}$
7	$\begin{bmatrix} 1 & 0 & -\sqrt{3} \\ 0 & 1 & -\dfrac{\sqrt{3}}{\sqrt{2}} \end{bmatrix}$	–	1.8439	$\begin{bmatrix} 0.5455 & 0.3857 & 0.3149 \\ 0.3857 & 0.2727 & 0.2227 \\ 0.3149 & 0.2227 & 0.1818 \end{bmatrix}$
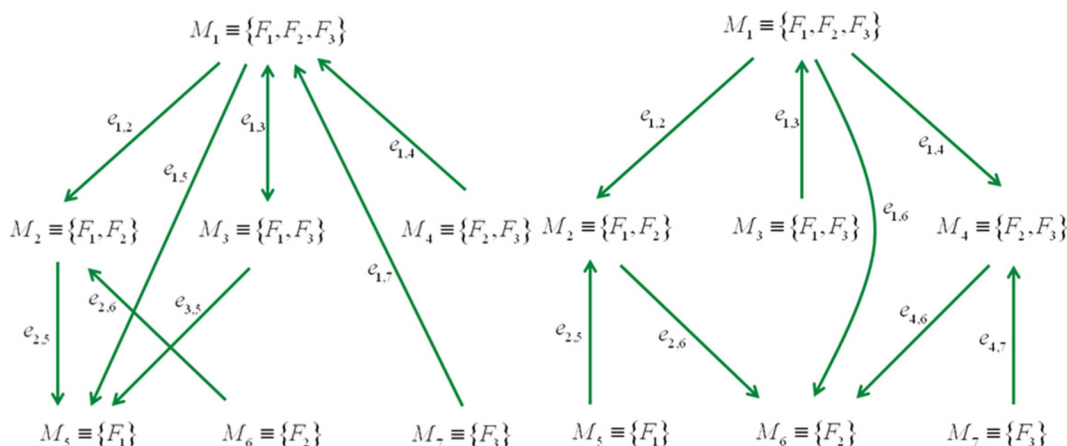
Figure A2. Flux maps showing interaction between different domains under different growth rates. (a) Flux map when the growth rate vector is pointing toward M_5 and (b) flux map when growth rate vector is pointing toward M_6.

Table A2. Incoming Fluxes J_s^+ from Higher Domains and the Resulting Feed Rate $\dot{B}_s$ for Potash Alum

s	J_s^+	$\dot{B}_s$
1	$\{\phi\}$	0
2	$\{1\}$	$\mathbf{A}_1\mathbf{P}_1\dot{\mathbf{H}}\delta(\mathbf{A}_1\mathbf{h})n(\mathbf{h},t)\big\|_{\mathbf{A}_1\mathbf{h}=0^-}$
3(1)	$\{2\}$	$\mathbf{A}_2\mathbf{P}_1\dot{\mathbf{H}}\delta(\mathbf{A}_2\mathbf{h})n(\mathbf{h},t)\big\|_{\mathbf{A}_2\mathbf{h}=0^-}$
3(2)	$\{\phi\}$	0
3(3)	$\{\phi\}$	0
4	$\{\phi\}$	0
5	$\{6,8\}$	$\mathbf{A}_6\mathbf{P}_2\dot{\mathbf{H}}\delta(\mathbf{A}_6\mathbf{h})n(\mathbf{h},t)\big\|_{\substack{\mathbf{D}_5\mathbf{h}=0\\\mathbf{A}_6\mathbf{h}=0^-}} + \mathbf{A}_8\mathbf{P}_3\dot{\mathbf{H}}\delta(\mathbf{A}_8\mathbf{h})n(\mathbf{h},t)\big\|_{\substack{\mathbf{D}_5\mathbf{h}=0\\\mathbf{A}_8\mathbf{h}=0^-}}$
6	$\{\phi\}$	0
7	$\{\phi\}$	0

Table A3. Incoming Fluxes J_s^- from Lower Domains and Flux Balance Equations for Potash Alum

s	J_s^-	Flux Balance Equations
1	$\{3,5\}$	$\mathbf{P}_1\dot{\mathbf{H}}n(\mathbf{h},t)\big\|_{\mathbf{A}_3\mathbf{h}=0^-} = \mathbf{P}_{3(2)}\dot{\mathbf{H}}n(\mathbf{h},t)\big\|_{\mathbf{D}_{3(2)}\mathbf{h}=0}$ $\mathbf{P}_1\dot{\mathbf{H}}n(\mathbf{h},t)\big\|_{\mathbf{A}_5\mathbf{h}=0^-} = \mathbf{P}_5\dot{\mathbf{H}}n(\mathbf{h},t)\big\|_{\mathbf{D}_5\mathbf{h}=0}$
2	$\{7\}$	$\mathbf{P}_2\dot{\mathbf{H}}n(\mathbf{h},t)\big\|_{\substack{\mathbf{D}_6\mathbf{h}=0\\\mathbf{A}_7\mathbf{h}=0^-}} = \mathbf{P}_6\dot{\mathbf{H}}n(\mathbf{h},t)\big\|_{\mathbf{D}_6\mathbf{h}=0}$
3(1)	$\{4\}$	$\mathbf{P}_{3(1)}\dot{\mathbf{H}}n(\mathbf{h},t)\big\|_{\substack{\mathbf{D}_{3(1)}\mathbf{h}=0\\\mathbf{A}_{3(2)}\mathbf{h}=0^-}} = \mathbf{P}_{3(3)}\dot{\mathbf{H}}n(\mathbf{h},t)\big\|_{\mathbf{D}_{3(3)}\mathbf{h}=0}$
3(2)	$\{\phi\}$	–
3(3)	$\{\phi\}$	–
4	$\{\phi\}$	–
5	$\{\phi\}$	–
6	$\{\phi\}$	–
7	$\{\phi\}$	–

morphology graph, and morphology domain for any material. The matrix $\mathbf{D}_s$ corresponds to the linear inequalities associated with the edge $e_{1,s}$ and the matrix $\mathbf{G}_s$ can be formed using elements of $\dot{\mathbf{H}}$. For the sake of clarity in the foregoing analysis, a fixed growth rate vector $\dot{\mathbf{H}} = \begin{bmatrix} 1 & 1.5 & 1.8 \end{bmatrix}^T$ of arbitrary units is chosen in the direction pointing toward M_5 (the cubic morphology) in morphology domain. The projection matrix can be computed using eq 12. Table A1 shows the specific values of $\mathbf{D}_s$, $\mathbf{G}_s$, α_s, and $\mathbf{P}_s$ for potash alum. A morphology graph (shown in Figure A1) analogous to Figure 2a can be constructed using first-order edges such that each set is connected forwardly with its subset. The vertices and edges of

the morphology graph of potash alum in Figure A1 are related using eq 15 as follows:

$$
\begin{bmatrix} M_1 \\ M_2 \\ M_{3(1)} \\ M_{3(2)} \\ M_{3(3)} \\ M_4 \\ M_5 \\ M_6 \\ M_7 \end{bmatrix} = \begin{bmatrix} -1 & -1 & -1 & -1 & -1 & 0 & 0 & 0 & 0 & 0 & 0 \\ 1 & 0 & 0 & 0 & 0 & -1 & -1 & 0 & 0 & 0 & 0 \\ 0 & 1 & 0 & -1 & 0 & 0 & 0 & -1 & 0 & 0 & 0 \\ 0 & 0 & 1 & -1 & 0 & 0 & 0 & 0 & -1 & 0 & 0 \\ 0 & 1 & 1 & 1 & 0 & 0 & 0 & 0 & 0 & 0 & 0 \\ 0 & 0 & 0 & 0 & 1 & 0 & 0 & 0 & 0 & -1 & -1 \\ 0 & 0 & 0 & 0 & 0 & 1 & 0 & 1 & 0 & 0 & 0 \\ 0 & 0 & 0 & 0 & 0 & 0 & 1 & 0 & 0 & 1 & 0 \\ 0 & 0 & 0 & 0 & 0 & 0 & 0 & 0 & 1 & 0 & 1 \end{bmatrix} \begin{bmatrix} e_{1,2} \\ e_{1,3(1)} \\ e_{1,3(2)} \\ e_{1,3(3)} \\ e_{1,4} \\ e_{2,5} \\ e_{2,6} \\ e_{3,5} \\ e_{3,7} \\ e_{4,6} \\ e_{4,7} \end{bmatrix}
$$

(31)

The identification of J_s^+ and J_s^- is a function of growth rate vector $\dot{\mathbf{H}}$ which, for the sake of clarity, is fixed in the direction pointing toward M_5 (the cubic morphology) in the morphology domain. The set of fluxes coming from higher domains J_s^+ and those coming from the lower domains J_s^- to the sth domain at given face-specific growth rates will create a flux map. The flux maps of potash alum at different growth rates are shown in Figure A2.

The set J_s^+ corresponding to Figure A2a and the feed rates $\dot{B}_s$ on the right-hand side of eq 18 are given in Table A2.

The set of fluxes J_s^- coming from lower domains are accounted by eq 21, which for potash alum are given in Table A3.

Notations

$\mathbf{A}$	matrix of normal vectors of the faces of morphology domain $[-]$
$\mathbf{A}_r$	submatrix of A associated with the rth edge of the morphology graph $[-]$
$\dot{B}_s$	feed coming to sth domain from other connected domains $[\mathrm{m}^{-m}\,\mathrm{s}^{-1}]$
c_0	initial concentration of solute $[\mathrm{mol\ m}^{-3}]$
c_{EG}	concentration of ethylene glycol $[\mathrm{mol\ m}^{-3}]$
c_{sat}	saturation concentration of solute $[\mathrm{mol\ m}^{-3}]$
C	morphology domain $[-]$
C_s	sth domain of the morphology domain $[-]$
$\mathbf{D}_s$	matrix of normal vectors defining the sth domain of the morphology domain $[-]$

$e_{s,s'}$	name of the edge in the morphology graph connecting vertices M_s and $M_{s'}$ $[-]$
$\mathbf{E}$	a column vector of first-order edges of the morphology graph $[-]$
F_i	name of the family of faces of the ith form $[-]$
$\mathbf{G}_s$	a bidiagonal matrix that relates the growth rates of real faces in sth domain of the morphology domain $[-]$
h_i	ith element of $\mathbf{h}$ $[m]$
$\mathbf{h}$	m-dimensional vector of perpendicular distances of crystal faces from crystal center. Also called as *h-vector* $[m]$
$\tilde{\mathbf{h}}$	n-dimensional vector of perpendicular distances of crystal faces from crystal center $[m]$
$\dot{\mathbf{H}}$	m-dimensional growth rate vector $[m\ s^{-1}]$
J_s^+	A set of first-order edges that will feed the sth domain from the higher domains $[-]$
J_s^-	A set of first-order edges that will feed the sth domain from the lower domains $[-]$
m	number of different forms (kinetically and geometrically similar) of faces $[-]$
M_i	ith set in the morphology set M representing a collection of different forms of faces $[-]$
M	$S \times 1$ vector of the vertices M_s
n	number of low-energy faces (F-faces) $[-]$
$n(\mathbf{h},t)$	number density in the morphology domain $[m^{-m}]$
$\mathbf{n}_i$	unit normal vector of the ith face $[-]$
N	null space $[-]$
$\mathbf{N}$	$n \times 3$-dimensional matrix of unit normal vectors of crystal faces $[-]$
P	power set containing 2^m subsets of $\{F_1, F_2, ..., F_m\}$ $[-]$
$\mathbf{P}_s$	projection matrix for the sth domain of the morphology domain $[-]$
$\mathbf{r}$	position vector in three-dimensional space $[m]$
R	number of edges in the morphology graph $[-]$
S	number of sets in the morphology set M $[-]$
t	time $[s]$
x_{EG}	mole fraction of ethylene glycol $[-]$
α_s	prefactor that scales the projected growth rates $\mathbf{P}_s\dot{\mathbf{H}}$ such that the real growth rates are unaltered $[-]$
$\delta(\mathbf{A},\mathbf{h})$	k-dimensional Dirac delta function $[m^{-k}]$
ρ	density of crystals $[kg\ m^{-3}]$
$\boldsymbol{\nu}_i$	ith ortho-normal basis vector of the null space of $\mathbf{D}_s$ $[-]$
$\boldsymbol{\mu}_i$	ith ortho-normal basis vector of the null space of $\mathbf{G}_s$ $[-]$
$\mathcal{R}^3$	three dimensional real space $[-]$
$\mathcal{R}_{+0}^m$	non-negative orthant of m-dimensional real space $[-]$
$\mathcal{R}_{+0}^n$	non-negative orthant of n-dimensional real space $[-]$

■ AUTHOR INFORMATION

Corresponding Author
*E-mail: ramkrish@purdue.edu.

Notes
The authors declare no competing financial interest.

■ REFERENCES

(1) Gibbs, J. W. On the equilibrium of heterogeneous substances. *Trans. Connecticut Acad. Arts Sci.* **1878**, 3, 343–524.

(2) Curie, P. Sur la formation des cristaux et sur les constantes capillaires de leurs différentes faces. *Bull. Soc. Franc. Mineral* **1885**, 8, 145–150.

(3) Wulff, G. Zur Frage der Geschwindigkeit des Wachstums und der Auflosung der Krystallflachen. *Z. Krystallogr. Mineral* **1901**, 34, 449.

(4) Hilton, H. *Mathematical Crystallography and the Theory of Groups of Movements*; The Clarendon Press: Gloucestershire, 1903.

(5) Liebmann, H. Der Curie-Wulff'sche Satz über Combinationsformen von Krystallen. *Z. Krystallogr. Mineral.* **1914**, 53, 171–177.

(6) von Laue, M. Der Wulffsche Satz für die Gleichgewichtsform von Kristallen. *Z. Kristallogr.* **1943**, 105, 124–133.

(7) Dinghas, A. Über einen geometrischen Satz von Wulff für die Gleichgewichtsform von Kristallen. *Z. Kristallogr.* **1944**, 105, 304–314.

(8) Taylor, J. E. Crystalline variational problems. *Bull. Amer. Math. Soc.* **1978**, 84 (4), 568–588.

(9) Cabrera, N. The Equilibrium of Crystal Surfaces. *Surf. Sci.* **1964**, 2, 320–345.

(10) Herring, C., The use of classical macroscopic concepts in surface energy problems. In *Structure and Properties of Solid Surfaces*; Gomer, R., Smith, C. S., Ed.; University of Chicago Press: Chicago, 1953; pp 5–72.

(11) Mullins, W. Metal surfaces: structure, energetics and kinetics. *Am. Soc. Metals, Metals Park, Ohio* **1963**, 17–66.

(12) Winn, D.; Doherty, M. F. Modeling crystal shapes of organic materials grown from solution. *AIChE J.* **2000**, 46 (7), 1348–1367.

(13) Frank, F. On the kinematic theory of crystal growth and dissolution processes. In *Growth and Perfection of Crystals*; Doremus, R. H., Roberts, B. W. , Turnbull, D., Eds.; Wiley: New York, 1958; pp 411–419.

(14) Cahn, J.; Taylor, J.; Handwerker, C. Evolving crystal forms: Frank's characteristics revisited. *Sir Charles Frank, OBE, ERS: An Eightieth Birthday Tribute*; Chambers, R. G. et al.), Adam Hilger: New York, 1991, 88–118.

(15) Taylor, J. E.; Cahn, J. W.; Handwerker, C. A. Geometric models of crystal growth. *Acta Metall. Mater.* **1992**, 40 (7), 1443–1474.

(16) Chernov, A. The kinetics of the growth forms of crystals. *Sov. Phys. Cryst.* **1963**, 7, 728–730.

(17) Hartman, P.; Perdok, W. On the relations between structure and morphology of crystals. I. *Acta Crystallogr.* **1955**, 8 (1), 49–52.

(18) Hartman, P.; Perdok, W. On the relations between structure and morphology of crystals. II. *Acta Crystallogr.* **1955**, 8 (9), 521–524.

(19) Hartman, P.; Perdok, W. On the relations between structure and morphology of crystals. III. *Acta Crystallogr.* **1955**, 8 (9), 525–529.

(20) Bravais, A. *Etudes Cristallographiques*; Gauthier-Villars: France, 1866.

(21) Friedel, M. G. Études Sur la loi de Bravais. *Bull. Soc. Franc. Miner.* **1907**, 9.

(22) Donnay, J.; Harker, D. A new law of crystal morphology extending the law of Bravais. *Am. Mineral.* **1937**, 22 (5), 446–467.

(23) Volmer, M.; Marder, M. Zur Theorie der linearen Kristallisations-geschwindigkeit unterkuhlter Schemlzen und unterkuhlter fester Modifikationen. *Z. Phys. Chem.* **1931**, A154.

(24) Kaichew, R.; Stranski, I. N. Zur Theorie der linearen Kristallisationsgeschwindigkeit. *Z. Phys. Chem.* **1934**, A170.

(25) Burton, W.; Cabrera, N.; Frank, F. The growth of crystals and the equilibrium structure of their surfaces. *Philos. Trans. R. Soc. London. Ser. A* **1951**, 299–358.

(26) Chernov, A. The spiral growth of crystals. *Physics-Uspekhi* **1961**, 4 (1), 116–148.

(27) Boerrigter, S.; Josten, G.; Van De Streek, J.; Hollander, F.; Los, J.; Cuppen, H.; Bennema, P.; Meekes, H. MONTY: Monte Carlo crystal growth on any crystal structure in any crystallographic orientation; application to fats. *J. Phys. Chem. A* **2004**, 108 (27), 5894–5902.

(28) Johnsen, A. *Wachstum und Auflösung der Kristalle*; Wilhelm Engelmann: Leipzig, 1910; p 27.

(29) Borgstrom, L. H. Die geometrische Bedingung fur die Entstehung von Kombinationen. *Z. Kristallogr.* **1925**, 62.

(30) Alexandru, H. A macroscopic model for the habit of crystals grown from solutions. *J. Cryst. Growth* **1969**, 5 (2), 115−124.

(31) Kozlovskii, M. I. Kinetics of crystallization at constant temperature and supersaturation. *Kristallografiya* **1957**, 2.

(32) Szurgot, M.; Prywer, J. Growth velocities and disappearance of faces of crystals. *Cryst. Res. Technol.* **1991**, 26 (2), 147−153.

(33) Prywer, J. Three-dimensional model of faces disappearance in crystal habit. *J. Cryst. Growth* **1995**, 155 (3), 254−259.

(34) Prywer, J. Three-dimensional model of any shape face disappearance in crystal habit. *J. Cryst. Growth* **1996**, 158 (4), 568−575.

(35) Gadewar, S. B.; Doherty, M. F. A dynamic model for evolution of crystal shape. *J. Cryst. Growth* **2004**, 267 (1), 239−250.

(36) Zhang, Y.; Sizemore, J. P.; Doherty, M. F. Shape evolution of 3-dimensional faceted crystals. *AIChE J.* **2006**, 52 (5), 1906−1915.

(37) Chakraborty, J.; Singh, M. R.; Ramkrishna, D.; Borchert, C.; Sundmacher, K. Modeling of crystal morphology distributions. Towards crystals with preferred asymmetry. *Chem. Eng. Sci.* **2010**, 65 (21), 5676−5686.

(38) Reinhold, A.; Briesen, H. Convex Geometry for the Morphological Modeling and Characterization of Crystal Shapes. *Part. Part. Syst. Charact.* **2012**, 28, 37−56.

(39) Borchert, C.; Sundmacher, K. Efficient formulation of crystal shape evolution equations. *Chem. Eng. Sci.* **2012**, 84, 85−99.

(40) Singh, M. R.; Verma, P.; Tung, H.-H.; Bordawekar, S.; Ramkrishna, D. Screening crystal morphologies from crystal structure. *Cryst. Growth Des.* **2013**, DOI: 10.1021/cg400009m.

(41) Singh, M.; Verma, P.; Ramkrishna, D. MorphologyDomain: A Software for Crystal Morphology Screening, https://engineering.purdue.edu/~drops/softwares/MorphologyDomain.zip

(42) Ramkrishna, D. *Population Balances: Theory and Applications to Particulate Systems in Engineering*; Academic Press: New York, 2000.

(43) Cardew, P. The growth shape of crystals. *J. Cryst. Growth* **1985**, 73 (2), 385−391.

(44) Puel, F.; Marchal, P.; Klein, J. Habit transient analysis in industrial crystallization using two dimensional crystal sizing technique. *Chem. Eng. Res. Des.* **1997**, 75 (2), 193−205.

(45) Ma, D.; Tafti, D.; Braatz, R. High-resolution simulation of multidimensional crystal growth. *Ind. Eng. Chem. Res.* **2002**, 41 (25), 6217−6223.

(46) Kumar, S.; Ramkrishna, D. On the solution of population balance equations by discretization—I. A fixed pivot technique. *Chem. Eng. Sci.* **1996**, 51 (8), 1311−1332.

(47) Chakraborty, J.; Kumar, S. A new framework for solution of multidimensional population balance equations. *Chem. Eng. Sci.* **2007**, 62 (15), 4112−4125.

(48) Mahoney, A. W.; Ramkrishna, D. Efficient solution of population balance equations with discontinuities by finite elements. *Chem. Eng. Sci.* **2002**, 57 (7), 1107−1119.

(49) Gunawan, R.; Fusman, I.; Braatz, R. D. High resolution algorithms for multidimensional population balance equations. *AIChE J.* **2004**, 50 (11), 2738−2749.

(50) Zhang, Y.; Doherty, M. F. Simultaneous prediction of crystal shape and size for solution crystallization. *AIChE J.* **2004**, 50 (9), 2101−2112.

(51) Borchert, C.; Nere, N.; Ramkrishna, D.; Voigt, A.; Sundmacher, K. On the prediction of crystal shape distributions in a steady-state continuous crystallizer. *Chem. Eng. Sci.* **2009**, 64 (4), 686−696.

(52) Briesen, H. Simulation of crystal size and shape by means of a reduced two-dimensional population balance model. *Chem. Eng. Sci.* **2006**, 61 (1), 104−112.

(53) Ma, C. Y.; Wang, X. Z.; Roberts, K. J. Morphological population balance for modeling crystal growth in face directions. *AIChE J.* **2008**, 54 (1), 209−222.

(54) Wang, X. Z.; Ma, C. Y. Morphological population balance model in principal component space. *AIChE J.* **2009**, 55 (9), 2370−2381.

(55) Wan, J.; Wang, X. Z.; Ma, C. Y. Particle shape manipulation and optimization in cooling crystallization involving multiple crystal morphological forms. *AIChE J.* **2009**, 55 (8), 2049−2061.

(56) Singh, M. R.; Chakraborty, J.; Nere, N.; Tung, H. H.; Bordawekar, S.; Ramkrishna, D. Image-Analysis-Based Method for 3D Crystal Morphology Measurement and Polymorph Identification Using Confocal Microscopy. *Cryst. Growth Des.* **2012**, 12 (7), 3735−3748.

(57) Oullion, M.; Puel, F.; Fevotte, G.; Righini, S.; Carvin, P. Industrial batch crystallization of a plate-like organic product. In situ monitoring and 2D-CSD modelling. Part 2: Kinetic modelling and identification. *Chem. Eng. Sci.* **2007**, 62 (3), 833−845.

(58) Kee, N. C. S.; Arendt, P. D.; Goh, L. M.; Tan, R. B. H.; Braatz, R. D. Nucleation and growth kinetics estimation for L-phenylalanine hydrate and anhydrate crystallization. *CrystEngComm* **2011**, 13 (4), 1197−1209.

(59) Ma, C. Y.; Wang, X. Z. Model identification of crystal facet growth kinetics in morphological population balance modeling of l-glutamic acid crystallization and experimental validation. *Chem. Eng. Sci.* **2012**, 70, 22−30.

(60) Larsen, P.; Rawlings, J.; Ferrier, N. Model-based object recognition to measure crystal size and shape distributions from in situ video images. *Chem. Eng. Sci.* **2007**, 62 (5), 1430−1441.

(61) Borchert, C.; Sundmacher, K. Morphology evolution of crystal populations: Modeling and observation analysis. *Chem. Eng. Sci.* **2012**, 70, 87−98.

(62) Lipschutz, S. *Schaum's Outline of Theory and Problems of Set Theory and Related Topics*; McGraw-Hill: New York, 1964.

(63) Alexandrov, A. D. *Convex polyhedra*; Springer: New York, 2005.

(64) Rhee, H. K.; Aris, R.; Amundson, N. R. *First-Order Partial Differential Equations*; Dover Publications: Mineola, NY, 2001; Vol. 2.

(65) Kuznetsov, V.; Okhrimenko, T.; Rak, M. Growth promoting effect of organic impurities on growth kinetics of KAP and KDP crystals. *J. Cryst. Growth* **1998**, 193 (1), 164−173.